PHYSICAL SCIENCES

Dramatic influence of patchy attractions on short-time protein diffusion under crowded conditions

Saskia Bucciarelli,[1] Jin Suk Myung,[1,2] Bela Farago,[3] Shibananda Das,[2] Gerard A. Vliegenthart,[2] Olaf Holderer,[4] Roland G. Winkler,[2] Peter Schurtenberger,[1] Gerhard Gompper,[2] Anna Stradner[1,5]*

In the dense and crowded environment of the cell cytoplasm, an individual protein feels the presence of and interacts with all surrounding proteins. While we expect this to strongly influence the short-time diffusion coefficient D_s of proteins on length scales comparable to the nearest-neighbor distance, this quantity is difficult to assess experimentally. We demonstrate that quantitative information about D_s can be obtained from quasi-elastic neutron scattering experiments using the neutron spin echo technique. We choose two well-characterized and highly stable eye lens proteins, bovine α-crystallin and γ_B-crystallin, and measure their diffusion at concentrations comparable to those present in the eye lens. While diffusion slows down with increasing concentration for both proteins, we find marked variations that are directly linked to subtle differences in their interaction potentials. A comparison with computer simulations shows that anisotropic and patchy interactions play an essential role in determining the local short-time dynamics. Hence, our study clearly demonstrates the enormous effect that weak attractions can have on the short-time diffusion of proteins at concentrations comparable to those in the cellular cytosol.

INTRODUCTION

The complex machinery of life in the interior of cells is determined by the dynamical properties of proteins. Proteins move in the dense and crowded environment of the cell cytoplasm, where an individual protein feels the presence and interaction potential of all surrounding proteins (*1*–*5*). We thus expect that direct and hydrodynamic interactions will strongly alter diffusion already on length scales comparable to or smaller than the average distance between them, which is essential for numerous cellular processes like protein reactions, recognition, and signal transduction (*6*–*8*). Thus, there is a need to extend the commonly conducted investigations of protein interactions in dilute solutions and to tackle the problem of measuring, understanding, and predicting the diffusion of proteins under crowded conditions, as prevailing in the cell cytosol. Previous studies mainly focused on the long-time diffusion of proteins over macroscopic distances and clearly demonstrate the slowing-down effect of a dense environment (*9*). In contrast, measuring short-time diffusion over dimensions comparable to the protein size poses particular challenges for the experimental analysis of protein dynamics, and only a few techniques, such as neutron spin echo (NSE) (*10*), are available to provide this information.

There are several NSE studies that report protein diffusion in crowded solutions, and the respective data are interpreted on the basis of colloid theories to include interaction effects between proteins at high densities in the strive to explain the experimental observations (*11*–*15*). However, the currently available range of investigated concentrations and well-characterized proteins is still limited, and the analysis has primarily focused on understanding the effects of excluded volume and (repulsive) screened Coulomb interactions on short-time diffusion. This is in stark contrast to the fact that numerous globular proteins exhibit a phase diagram that is very similar to that found in colloids with weak short-range attractions (*16*–*18*), which indicates the importance of attractive interactions. Thus, we have performed a systematic investigation of the short-time diffusion coefficient D_s of two small globular lens proteins known to have either hard sphere-like repulsion (α-crystallin) (*19*) or weak short-range attractions (γ_B-crystallin) (*18*, *20*, *21*) by NSE.

The hard sphere-like protein α-crystallin is a quite polydisperse multisubunit protein with an average molecular weight of about 8×10^5, an average hydrodynamic radius of about $R_h = 9.6$ nm, and a polydispersity of about 20% (*19*). It has been shown to behave like ideal hard spheres all the way up to the glass transition occurring at a volume fraction of $\phi = 0.58$. On the other hand, γ_B-crystallin is a monodisperse monomeric protein with a molecular weight of around 21,000 and a hydrodynamic radius $R_h = 2.3$ nm (*20*). Its solution structure and phase diagram are well reproduced by a coarse-grained potential, combining a hard core repulsion and a weak short-range attraction and assuming either a spherical or a weakly elliptical shape (*18*, *20*).

RESULTS

NSE measurements of protein diffusion

Given the very limited use of NSE in studies of dense protein solutions, we first briefly summarize the type of information obtained in quasi-elastic scattering (QES) experiments and the expectations for dense protein solutions based on analogies with colloid models. QES techniques, such as dynamic light scattering (DLS) or NSE, probe the dynamics of concentration or density fluctuations on length scales d, where d is determined by the magnitude of the inverse scattering vector q, that is, $d \approx 2\pi/q$, with $q = (2\pi/\lambda)\sin(\theta/2)$, where λ is the wavelength of the incident radiation and θ is the scattering angle (*22*). Thus, QES provides a q-dependent effective diffusion coefficient $D(q)$. For dense particle systems, we then expect to find dynamical regimes as sketched and described schematically in Fig. 1.

For the suspensions of hard sphere-like particles, the dynamical behavior is well characterized and known from a number of experimental, theoretical, and simulation studies for volume fractions ϕ all the way up to the glass transition at $\phi_g \approx 0.58$ (*23*). On length scales

[1]Division of Physical Chemistry, Department of Chemistry, Lund University, Naturvetarvägen 16, SE-221 00 Lund, Sweden. [2]Theoretical Soft Matter and Biophysics, Institute of Complex Systems and Institute for Advanced Simulation, Forschungszentrum Jülich, D-52425 Jülich, Germany. [3]Institut Laue-Langevin (ILL), F-38042 Grenoble Cedex 9, France. [4]Jülich Centre for Neutron Science (JCNS) at Heinz Maier-Leibnitz Zentrum (MLZ), Forschungszentrum Jülich GmbH, Lichtenbergstr. 1, D-85748 Garching, Germany. [5]Department of Chemistry, University of Fribourg, Chemin du Musée 9, CH-1700 Fribourg, Switzerland.
*Corresponding author. Email: anna.stradner@fkem1.lu.se

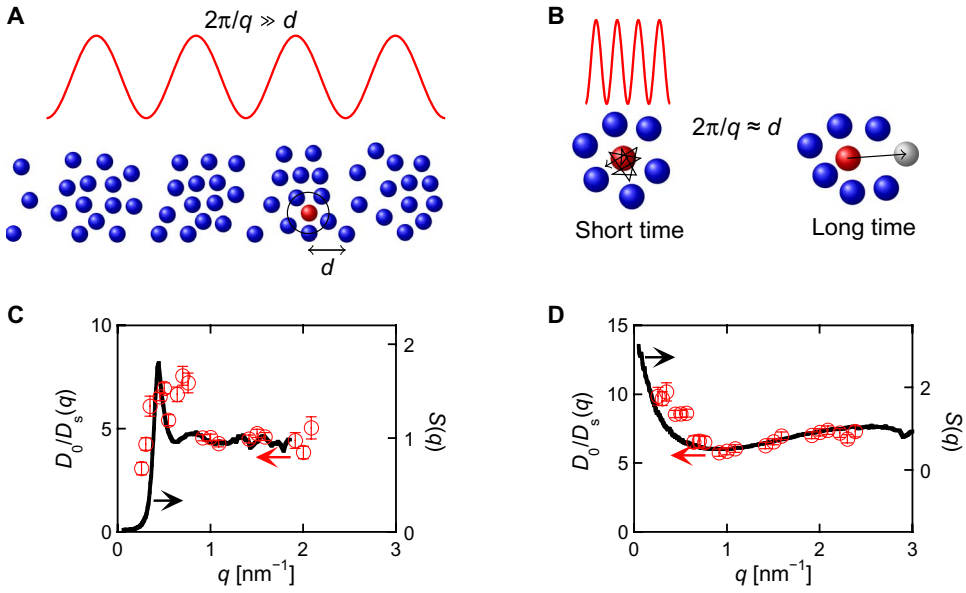

Fig. 1. Dynamics of crowded solutions probed by NSE. (**A** and **B**) Schematic description of the link between the scattering vector q and the length scale of the density fluctuations probed. Shown are the large-scale fluctuations probed at low q (A) and local dynamics probed at the nearest-neighbor length d (B), where for dense hard sphere systems, two well-separated mechanisms emerge (see text for details). (**C** and **D**) Comparison between the dynamic [$D_0/D(q)$, open symbols, left axis] and the static [$S(q)$, from SAXS, solid line, right axis] structure factor for α-crystallin solutions at $\phi = 0.50$ and $T = 298$ K (C) and for γ_B-crystallin solutions at $\phi = 0.16$ and $T = 308$ K (D).

much larger than the nearest-neighbor distance $d \gg 2a$ (or $q \ll \pi/a$), where a is the particle radius, QES measures collective diffusion, which for hard spheres is known to accelerate at short times, reflecting the reduced osmotic compressibility of repulsive systems. However, at distances corresponding to the nearest-neighbor distance $d \approx 2a$, QES probes the relaxation of the dominant local structure determined by the nearest-neighbor cage. The corresponding diffusion coefficient $D(q^*)$, where $q^* \approx 2\pi/d$ is the position of the first peak in the static structure factor $S(q)$, then exhibits increasingly separated short- and long-time processes that are qualitatively described by local diffusion or "rattling" in the nearest-neighbor cage, followed by cage opening and diffusion out of the cage. Here, the limits of short-time diffusion are typically bracketed by the time scale $\tau_H \approx R^2\rho/(\eta\phi)$, where hydrodynamic interactions arise, and by the structural relaxation time $\tau_I \approx R^2/D_0$, with $\tau_H \ll t \ll \tau_I$ (*23*). Here, R is the particle radius, ρ is the solvent density, η is the solvent viscosity, and ϕ is the particle volume fraction. For our protein solutions, this results in a time range of about 50 ps $\ll t \ll$ 100 ns for γ_B-crystallin and about 500 ps $\ll t \ll$ 5 μs for α-crystallin.

Over the full accessible q-range, we expect that the q dependence of the rescaled short-time diffusion coefficient $D_s(q)/D_0$ primarily reflects the q-dependent static structure factor $S(q)$ following $D_s(q) = D_0H(q)/S(q)$, where D_0 is the ideal diffusion coefficient of a noninteracting protein, modified by the hydrodynamic function $H(q)$, which captures the effect of hydrodynamic interactions (*23*). However, it is important to point out that hydrodynamic interactions strongly influence the magnitude of $D_s(q)$ (*6*, *24*). The close relationship between $D_s(q)$ and $S(q)$ is seen in the NSE experiments with the hard sphere-like protein α-crystallin shown in Fig. 1C, where $D_0/D_s(q)$ and $S(q)$ [from small-angle x-ray scattering (SAXS)] are shown for a volume fraction of $\phi = 0.50$ as a function of q.

For systems with attractive interactions, our current knowledge is much more limited. The data displayed in Fig. 1D demonstrate that $D_0/D_s(q)$ obtained for γ_B-crystallin at a volume fraction of $\phi = 0.16$, which is located very close to the critical volume fraction $\phi_c = 0.154$ (*22*), again follows $S(q)$. However, the qualitative q dependence is significantly different, reflecting the distinctly different form of $S(q)$ for attractive systems. The weak short-range attractions found in many globular proteins lead to a liquid-liquid phase separation at low temperatures T, and thus, the collective dynamics is often dominated by a critical slowing down due to the presence of a nearby critical point or spinodal (*20*). Thus, the collective dynamics probed at $q \ll q^*$ is expected to be slowed down, which is indeed seen for the low-q values in Fig. 1D. However, at the weakly pronounced nearest-neighbor peak (at $q^* \approx 2$ to 2.5 nm^{-1}, corresponding to a protein-protein distance of about 2.5 to 3 nm), contributions from critical slowing down are absent.

The markedly different concentration-dependent dynamical behavior on the nearest-neighbor length scale of the two proteins is reflected in the rescaled diffusion coefficient $D_s(q^*)/D_0$, as displayed in Fig. 2. For α-crystallin, Fig. 2A demonstrates that the measured $D_s(q^*)/D_0$ closely follows the theoretical prediction for hard spheres. This indicates that for hard sphere-like proteins, short-time diffusion on these length scales will slow down considerably in crowded solutions due to caging originating from neighboring proteins. Most importantly, the α-crystallin data in Fig. 2A indicate that colloid models quantitatively predict protein diffusion on these length scales over a broad concentration range. Knowing that the microstructure on length scales $d \approx 2\pi/q^*$ does not markedly change between hard sphere-like and weakly attractive particles, and following "common knowledge" that hydrodynamic interactions should be dominant for short-time diffusion, it is then tempting to use the hard sphere results also as a general guideline to estimate short-time diffusion on these length scales for other proteins, such as γ_B-crystallin (*6*). If we were able to validate the applicability of a hard sphere model to reasonably describe the concentration dependence of local short-time diffusion of proteins in a crowded environment, in general,

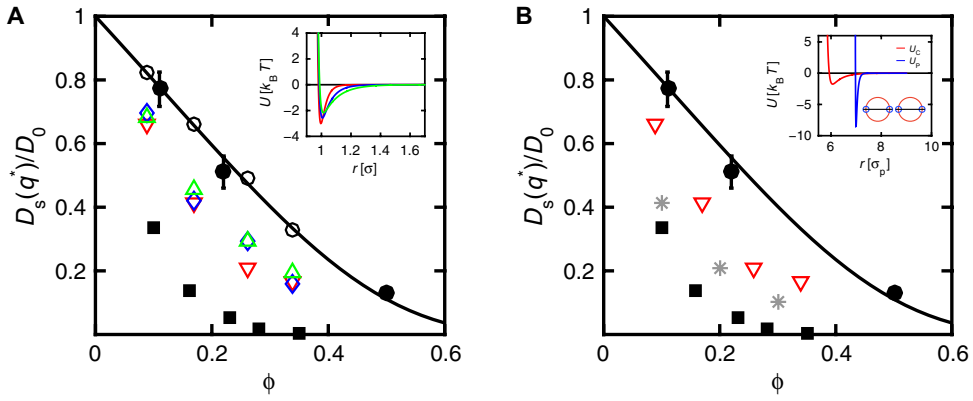

Fig. 2. Concentration dependence of the rescaled short-time diffusion at the nearest-neighbor distance $D_s(q^*)/D_0$. Comparison between the experimentally determined values [α-crystallin (filled black circles) and γ_B-crystallin (filled black squares)] and the computer simulation (open black circles) and theoretical (black line) (*23*) results for hard spheres. Moreover, computer simulation results are shown in (**A**) for the centrosymmetric potential given by Eq. 1 with the parameters $b = 30$, $\varepsilon/\varepsilon_r = 3.95$ (open inverse red triangles), $b = 15$, $\varepsilon/\varepsilon_r = 3.45$ (open blue diamonds), and $b = 9$, $\varepsilon/\varepsilon_r = 2.8$ (open green triangles), and in (**B**), the patchy particle model with $b = 15$, $\varepsilon/\varepsilon_r = 2.5$, and $b_p = 15$, $\varepsilon_p/\varepsilon_r = 9.5$ and $\sigma/\sigma_p = 6$ (gray stars). In addition, the results for the centrosymmetric potential of (A) (open inverse red triangles) are displayed for comparison. Error bars are plotted for the NSE data of both proteins and are smaller than the symbols for all the γ_B-crystallin samples and the α-crystallin sample at the highest concentration. The insets show the respective potentials.

this would allow us to directly use the data on protein-protein reactions and other cellular processes obtained at very dilute conditions in typical test tube experiments and correct them for crowding effects on diffusion.

However, surprisingly, our experiments suggest a drastically different dynamical behavior. Figure 2A shows that $D_s(q^*)/D_0$ for γ_B-crystallin markedly slows down with increasing concentration and decreases by almost three orders of magnitude already at a volume fraction of $\phi = 0.35$, which is far below close packing. The concentration effect is much more pronounced than that predicted by hard sphere theory or seen for α-crystallin.

Computer simulations of attractive particles

To shed light on the mechanisms responsible for the enormous slowing down of the γ_B-crystallin dynamics, we performed mesoscale hydrodynamic simulations by combining molecular dynamics simulations of the proteins with the multiparticle collision (MPC) dynamics approach for the embedding fluid (*25*, *26*). Hence, our simulations include thermal fluctuations and hydrodynamic interactions. Two models are considered for the protein-protein interactions. In the first model, we use a centrosymmetric weakly attractive short-range effective pair potential

$$U_c(r) = -\varepsilon\left(\frac{\sigma}{r}\right)e^{-b\left(\frac{r}{\sigma}-1\right)} + \varepsilon_r\left(\frac{\sigma}{r}\right)^{96} \quad (1)$$

where σ denotes the diameter of the spherical particle and r is the center-to-center distance between particles. The first term describes a short-range Yukawa attraction, where ε is the interaction strength and b is the screening parameter characterizing the interaction range, such that a larger b leads to a smaller range of attractive interaction. The second term models the hard core repulsion due to excluded volume interactions. For the temperature, we set $k_BT/\varepsilon_r = 1$. In the second model, we explore the effect of anisotropic interactions and take into account directional or patchy interactions. In practice, we add two patches diametrically arranged on the colloid surface, and model the patch-patch interaction with the short-range attractive pair potential of Eq. 1 and the parameters ε_p, σ_p, and b_p.

The choice of a spherical model for γ_B-crystallin, despite the fact that its real shape is better described by an ellipsoid with an axial ratio of about 1.8 to 2, is motivated by earlier studies of Ando and Skolnick (*6*) and Roosen-Runge *et al.* (*24*). They investigated the effect of moderate geometrical anisotropy based on the known molecular shapes of globular proteins comparable to γ_B-crystallin and concluded that the effective sphere models together with the corresponding interaction potentials are indeed reasonable approximations for analyzing diffusion in crowded solutions.

To relate the location of the simulated systems in the resulting phase diagram to the experimental conditions, we have chosen the rescaled second virial coefficient $B_2^* = B_2/B_2^{HS}$, where B_2 is the second virial coefficient of the considered system and B_2^{HS} is that of a pure hard sphere system, as an effective temperature (*27*). Because patchy particles do not follow the extended law of corresponding states, valid for centrosymmetric potentials, we compare the various systems for similar $\Delta B_2^* = (B_2^* - B_{2,cr}^*)/|B_{2,cr}^*|$, where $B_{2,cr}^*$ is the value of B_2^* at the critical temperature. For a given range of b of the attractive potential, ε was chosen such that ΔB_2^* is between 0.1 and 0.2, comparable to the experiments. The actual values of B_2^* are listed in Table 1. As has been observed before in colloidal systems with patchy interactions (*28*), the values for $B_{2,cr}^*$ are significantly smaller than those of isotropically interacting colloids. Our $B_{2,cr}^*$ value calculations for the model with centrosymmetric and patch interactions show that the combined effect leads to a $B_{2,cr}^*$ value, which is in between those of pure centrosymmetric and patchy interactions (compare Table 1). Note that additional experiments have shown that $D_s(q^*)/D_0$ for γ_B-crystallin is almost completely independent of temperature for a range of 298 K ≤ T ≤ 308 K, that is, for a range of $0.1 \le \Delta B_2^* \le 0.5$, thus indicating that the exact choice of B_2^* is not critical as long as the sample is in the one-phase region above the coexistence curve for liquid-liquid phase separation.

In the case of the centrosymmetric potential, we have used several combinations of ε and b to explore the effect of the range of the weak attraction on the resulting short-time diffusion coefficient. Figure 2A summarizes the results from these simulations for three pairs of parameters ($b = 30$ and $\varepsilon/\varepsilon_r = 3.95$, $b = 15$ and $\varepsilon/\varepsilon_r = 3.45$, and $b = 9$ and

$\varepsilon/\varepsilon_r = 2.8$, respectively). The shape of the potential is displayed in the inset in Fig. 2A. In addition, results for pure hard sphere fluids are shown as a benchmark to demonstrate the quantitative agreement between simulations and available theoretical predictions (*23*) for such systems. Evidently, the attractive interactions result in a short-time dynamics that is significantly slower than that of hard spheres. However, the centrosymmetric attractive interactions are obviously not able to even qualitatively reproduce the experimentally observed difference between α- and γ_B-crystallin. Moreover, a variation of the range and strength of the attraction (while maintaining a similar distance to the critical temperature, that is, a similar ΔB_2^*) has only a minor effect on the resulting value of the short-time diffusion coefficient. It thus seems clear that a simple centrosymmetric short-range attraction consistent with the overall phase diagram is not able to account for the marked slowing down of the short-time diffusion experimentally observed for γ_B-crystallin. Here, note that attempting to use a centrosymmetric potential compatible with the phase diagram of γ_B-crystallin represents a considerable constraint on the choice of the potential, since for short-range attractive particles, the critical concentration for liquid-liquid phase separation depends on the range of the attraction.

It has previously been suggested that interactions between γ_B-crystallins should not be described by a simple centrosymmetric pair potential, but a certain degree of patchiness should be included, similar to that found for other globular proteins (*20*, *29*). There are a number of structural features that can result in more directional or patchy attractions, such as a nonuniform charge distribution or hydrophobic patches on the protein surface. To elucidate the influence of such patchy interactions on the short-time diffusion of proteins, we apply the simple patchy colloid model mentioned above. We did not attempt to extract specific orientation-dependent interaction potentials or parameters using the known protein structure of γ_B-crystallins and to develop a coarse-grained, near-atomistic protein model. The model and the corresponding potentials are illustrated in the inset of Fig. 2B. To capture the characteristic features of directional patch-like interactions between proteins, the attraction between two patches is much stronger than the additional centrosymmetric potential. The diameter ratio of the colloid and patch "particle" is set to $\sigma/\sigma_p = 6$. The values of the full set of parameters are then fixed again such as to guarantee that the system is in the one-phase fluid regime.

Figure 2B shows that anisotropic, patchy, short-range attractions lead to a much stronger slowing down of the protein short-time dynamics than in the purely centrosymmetric case. The diffusion coefficients from the simulation are still larger than those extracted from the experiment, indicating that future work will be required to use the known molecular structure of γ_B-crystallin to arrive at a more refined model of the interaction potential. Nevertheless, Fig. 2B clearly demonstrates the importance of patchy attractions on the D_s of proteins in crowded solutions.

We obtain a qualitative understanding of the marked slowing down of short-time diffusion in the case of attractive patches from an inspection of the particle configurations found in the simulations. The snapshots of the colloid configurations shown in Fig. 3 illustrate that both types of attraction lead to the formation of temporary protein clusters (movies S1 and S2). However, they strongly differ in their average size and structure. For particles with isotropic attractions, the typical density fluctuations lead to the formation of rather compact clusters, where the largest cluster comprises only a small fraction of the colloids. Moreover, the cluster lifetime is relatively short, which is also in agreement with a simple estimate of the lifetime of temporary bonds (or particle escape time from the attractive well) created by the weak short-range attraction. An estimate of the escape time from the well using Kramer's theory [namely, $\tau_b \approx (\Delta^2/D_0)\exp(-\varepsilon/k_BT)$, where Δ is the width of the potential] leads to 5 ns $\lesssim \tau_b \lesssim$ 20 ns for the range of parameter values of the centrosymmetric potential. The addition of patchy attractions and the corresponding formation of much

Table 1. Values of the second viral coefficient B_2^*, $B_{2,cr}^*$, and the relative distance to the critical point for the models used in the simulations.

b	$\varepsilon/\varepsilon_r$	$\varepsilon_p/\varepsilon_r$	B_2^*	$B_{2,cr}^*$	$\Delta B_2^* = (B_2^* - B_{2,cr}^*)/\lvert B_{2,cr}^*\rvert$
9	2.8	0	−1.23	−1.38	0.11
15	3.45	0	−1.12	−1.29	0.13
30	3.95	0	−0.93	−1.20	0.23
15	2.5	9.5	−2.60	−2.87	0.09

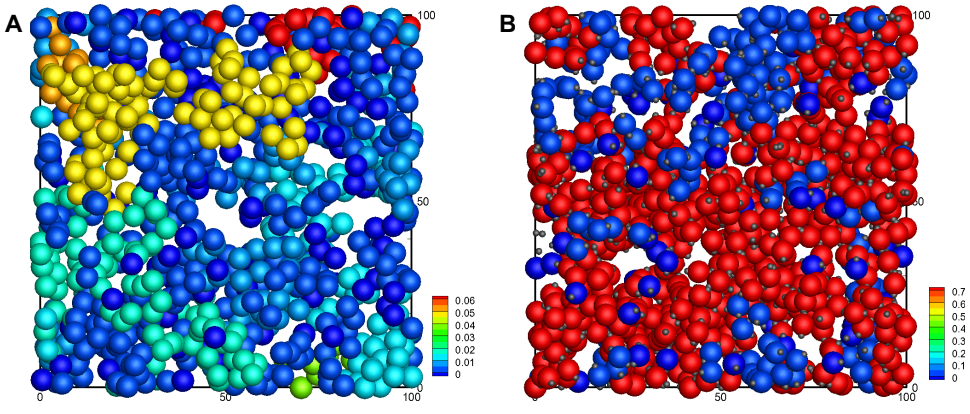

Fig. 3. Formation of transient clusters due to weak short-range attractions. Snapshots showing the configurations of particles at $\phi = 0.1$ for centrosymmetric attraction (**A**), and with two additional attractive patches (**B**). The color code corresponds to the size of the cluster, N_c/N, to which the particle belongs. Here, N_c is the number of particles in a cluster, and N is the total number of particles in the system. Note that clusters are only transient and that the cluster size fluctuates in time. See movies S1 and S2 for the two simulations.

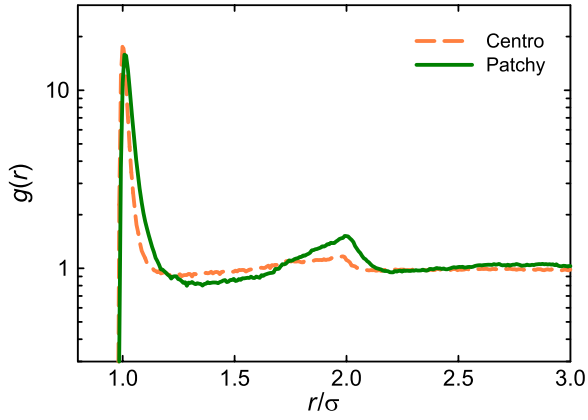

Fig. 4. Structural correlations in colloids with and without patchy interactions. Simulation results for the pair correlation function of colloids with centrosymmetric (dashed, orange) and additional patch interactions (solid, green) for $\phi = 0.1$. For the centrosymmetric potential, the parameters are $b = 30$, $\varepsilon/\varepsilon_r = 3.95$, and for the patchy system $b = 15$, $\varepsilon/\varepsilon_r = 2.5$, $b_p = 15$, $\varepsilon_p/\varepsilon_r = 9.5$, and $\sigma/\sigma_p = 6$.

larger and open network-like structures, where frequently a majority of particles form a single large cluster, yield long-lived temporary structures. Our simple estimate leads to lifetimes of $\tau_b \approx 200$ ns for the temporary bonds created by the attractive patches.

The formation of large and slowly relaxing clusters due to nonspecific attractive interactions in crowded protein solutions as a source of slowing down of long-time diffusion has already been pointed out in recent studies (*6*, *7*). Here, we now see that such interactions can also markedly slow down local diffusion and that this effect is strongly influenced by the existence of attractive patches.

A more quantitative analysis of these transient colloid structures provides additional insight on the origin of the slow down in the dynamics of patchy colloids compared to centrosymmetric interactions. Figure 4 displays pair correlation functions $g(r)$ for both types of interactions at a volume fraction $\phi = 0.1$. The correlation function exhibits a clear nearest-neighbor peak as well as a well-defined next nearest-neighbor peak of $g(r)$, which indicates the formation of clusters. This peak is more pronounced for the patchy colloid solution, and a more pronounced depletion between the first and second neighbors in the patchy colloid system was also obtained. Both aspects

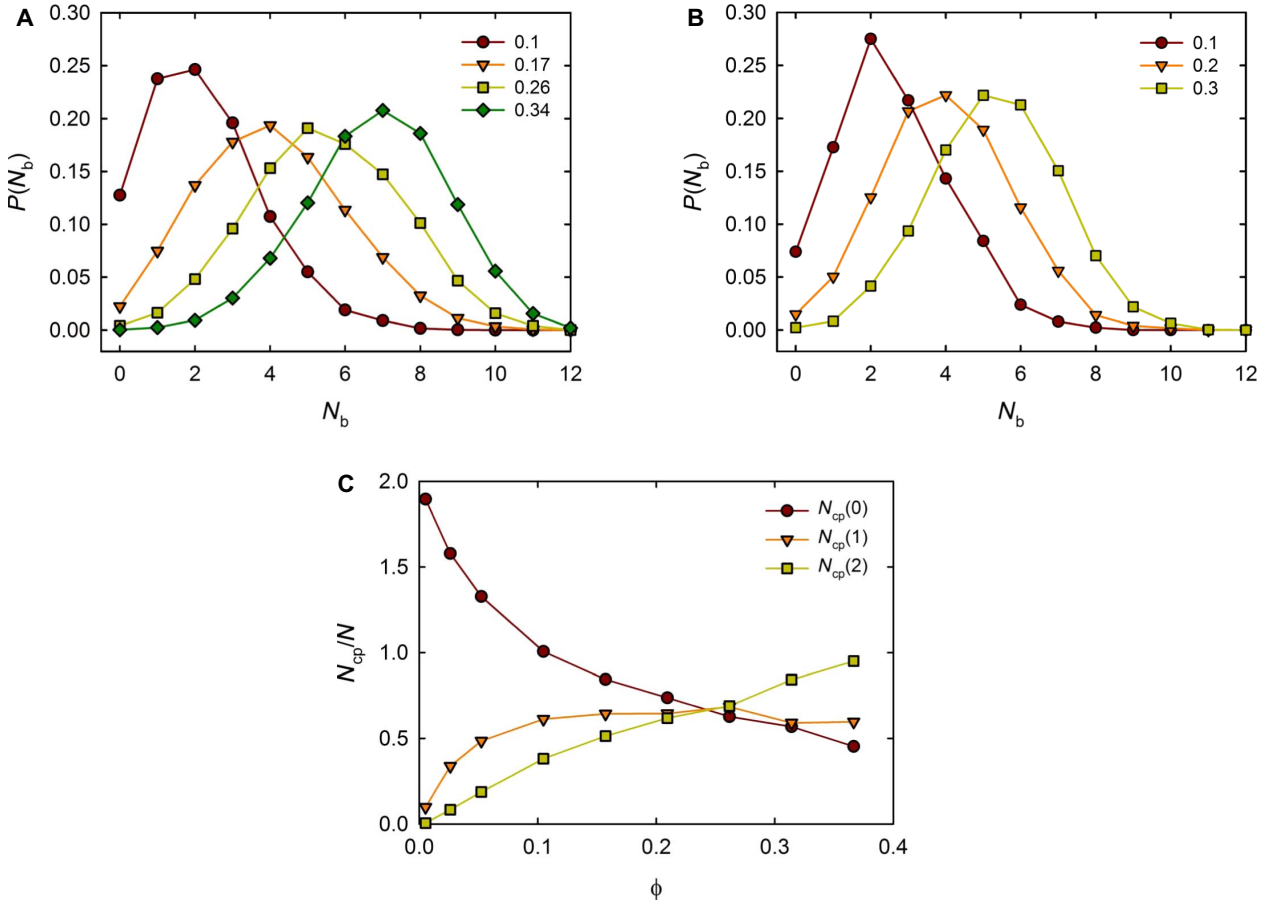

Fig. 5. Distribution functions of the number of neighbors N_b of a colloidal particle. (**A**) Distribution functions for colloids interacting solely by the centrosymmetric potential at the volume fractions $\phi = 0.1$, 0.17, 0.26, and 0.34. The potential parameters are $b = 30$ and $\varepsilon/\varepsilon_r = 3.95$. (**B**) Distribution functions for patchy colloids at $\phi = 0.1$, 0.2, and 0.3. The potential parameters are $b = 15$, $\varepsilon/\varepsilon_r = 2.5$, $b_p = 15$, and $\varepsilon_p/\varepsilon_r = 9.5$. Two colloids are considered as neighbors when their separation is smaller than the radial distance at the first minimum of the pair correlation function. (**C**) Relative number of patches $N_{cp}(n)$ in direct contact with each other as a function of the volume fraction, where n is the number of contacts. Zero corresponds to no patch contact, unity to one, etc. Two patches are in contact when their interaction energy is half the minimal energy of the patch-patch interaction potential.

point to distinct differences in the local structure, with significantly more prominent spatial correlations in the case of a patchy attraction.

These differences in the cluster structure are also reflected in the distribution of the number of nearest neighbors N_b of a particle, at least at low concentrations. The respective distribution functions are displayed in Fig. 5 (A and B). For both the nonpatchy and patchy colloids, the distribution functions at $\phi = 0.1$ exhibit a peak at $N_b = 2$, that is, aggregates of colloids with two neighbors dominate. However, the peak at $N_b = 2$ for the patchy system is more pronounced and indicates the preferred formation of strings due to patch-patch interactions. This is further supported by the connectivity of patches (compare Fig. 5C). With increasing volume fraction, the fraction of patches with one connection increases fast and saturates for $\phi > 0.1$. This corresponds to the formation of string-like structures and hence one-dimensional, long-lived aggregates. In addition, the fraction of patches with two connections (three colloids) is significant and exceeds that of all other connectivities above $\phi = 0.3$. Such links allow for branching of string-like structures. No patch connections by more than three colloids are present, which is prevented by the packing of colloids for the chosen patch size. At higher volume fractions, the differences in the cluster structure are less pronounced. Here, packing starts to dictate the local structure rather than specific interactions. The attraction between strings and parts of strings due to the additional isotropic potential enhances three-dimensional structure formation. Because the latter (isotropic) attraction is weaker than that for the nonpatchy systems, the appearing structures are more open and network-like. These temporary system-spanning networks are the origin of the marked slowing down of the short-time dynamics on the length and time scales measured in the NSE experiment. They also provide a likely explanation for the unusually slow collective dynamics and the existence of an arrest line at relatively low volume fractions of $\phi \approx 0.35$ for γ_B-crystallin solutions reported earlier (*20*).

DISCUSSION

Our findings show that the short-time diffusion of proteins over distances comparable to the average distance between nearest neighbors, crucial to many biological processes, is markedly slowed down at concentrations comparable to those found in the cytoplasm of living cells, compared to dilute solutions. This becomes particularly pronounced when the proteins exhibit short-range attractions, a feature common to many globular proteins. Moreover, our simulations also demonstrate that the presence of attractive patches on the protein surface can have a tremendous effect on $D_s(q^*)/D_0$, despite the fact that the overall strength of the effective pair potentials as characterized by B_2^* is comparable. To understand and predict the dynamics of crowded protein solutions, it is thus not sufficient to perform in vitro experiments under dilute conditions and use estimates of the overall strength of interparticle interactions together with standard colloid models. There is a clear need to extend the often-used simple colloid models and to incorporate more molecular features into such coarse-grained models when attempting to describe local short-time diffusion in crowded solutions (*6*, *7*).

The marked influence of weak attractive patches on local short-time diffusion not only is of considerable importance in the general case of crowding phenomena in cells and other dense protein environments but may also have direct implications for the specific system used in this study. Eye lens protein solutions have not only been investigated because of their role in cataract formation but their dynamics has also been recently investigated because of speculations that the occurrence of presbyopia (an age-related inability of the eye to focus on close objects)—a result of a gradual hardening of the eye lens—may be linked to an arrest or glass transition of the concentrated protein solutions that make up the interior of the fiber cells in the lens. While the molecular origins of such an age-related arrest transition are unknown, our simulations demonstrate that the additional presence of one or several attractive patches on the protein surface (for example, because of a local site mutation that creates an additional charged patch) may markedly alter the local and macroscopic dynamic properties and drive the solution into an arrested state. Thus, it will be interesting to study in more detail into the molecular properties of the various crystallins found in lenses with and without presbyopia.

MATERIALS AND METHODS

Protein purification and sample preparation

Proteins were purified from calf lenses, freshly obtained as a by-product from a local slaughterhouse. γ_B-Crystallin was isolated by size-exclusion chromatography of nuclear fractions on Superdex 200 prep grade, using 275 mM Na acetate buffer (pH 4.5), followed by cation exchange chromatography on SP Sepharose Fast Flow, using 275 mM Na acetate buffer (pH 4.8) and a 0 to 325 mM NaCl gradient. α-Crystallin was purified by size exclusion chromatography of cortical fractions on Superdex 200 prep grade, using 52.4 mM phosphate buffer (pH 7.1). As final solvent, 52.4 mM phosphate buffer in 100% D_2O including dithiothreitol (20 mM) and sodium azide (0.02 wt %) at pH 7.1, resulting in an ionic strength of about 130 mM, was used. Concentrations of protein solutions were determined by ultraviolet absorption spectroscopy at a wavelength of $\lambda = 280$ nm using the specific absorption coefficients $E^{1\%,280nm}_{\gamma B,1cm} = 2.18$ ml/mg·cm and $E^{1\%,280nm}_{\alpha,1cm} = 0.845$ ml/mg·cm (*19*, *30*, *31*). Volume fractions ϕ were calculated from the measured concentrations c using the formula $\phi = c \cdot \nu$, with ν being the voluminosity of the proteins ($\nu_\alpha = 1.7$ ml/g and $\nu_{\gamma B} = 0.7$ ml/g) (*21*, *32*).

Scattering experiments

SAXS measurements were performed on a pinhole camera (Ganesha 300 XL SAXS System, SAXSLAB) over a q-range of 0.03 to 3 nm^{-1}. NSE experiments were carried out at the spectrometers IN15 (*33*) at the Institut Laue-Langevin (ILL) in Grenoble, France, and J-NSE (*34*) operated by the Jülich Centre for Neutron Science (JCNS) at the Heinz Maier-Leibnitz Zentrum (MLZ) in Munich, Germany. We probed a q-range of 0.1 to 2.3 nm^{-1} and a Fourier time range between 0.03 and 600 ns. For α-crystallin, measurements were performed at either 25° or 35°C, but because α-crystallins behave like effective hard spheres, they do not exhibit any temperature dependence, and hence, we combined measurements performed at both temperatures without explicitly mentioning T. γ_B-Crystallin was measured at 35°C. The ideal diffusion coefficient D_0 required to normalize the measured values of $D_s(q)$ was determined as follows. D_0 is given by $D_0(T) = (k_B T)/[6\pi\,\eta(T) R_{h;0}]$, where k_B is the Boltzmann constant, $\eta(T)$ is the T-dependent solvent viscosity, and $R_{h;0}$ is the hydrodynamic radius of the noninteracting protein. For γ_B-crystallin, we obtained $R_{h;0} = 2.3$ nm from an extrapolation of the measured apparent hydrodynamic radius $R_{h;app}$ of a series of dilute samples to $\phi = 0$ using DLS. For α-crystallin, we used $R_{h;0} = 9.6$ nm (*19*).

Simulation approaches

Isotropic spherical colloids: The dynamical behavior of suspensions of the model lens protein γ_B-crystallin was investigated by mesoscale

hydrodynamic simulations. A protein is represented by a spherical shell composed of point particles, which are connected by suitable elastic bonds to maintain its shape (*35*). The colloids are embedded in the MPC fluid to account for hydrodynamic interactions. Calculations of colloid velocity correlation functions provide the correct hydrodynamic behavior on relevant length and time scales (*35*). Interactions between spherically symmetric colloids are described by the short-range attractive potential of Eq. 1. Anisotropic spherical colloids: To account for anisotropic, directional interactions, patches are placed on opposite sites on the colloid surface. In the latter case, the patch attraction is much stronger than the isotropic attraction by the central potential $\varepsilon_p/\varepsilon_c = 3.8$. The diameter ratio of colloid and patch particle was set to $\sigma/\sigma_p = 6$.

From the simulations, we calculated intermediate scattering functions (ISFs) $S(q,t)$ and extracted a short-time diffusion coefficient $D_s(q^*)$ from an exponential decay fit to the ISFs at a q value of $q^*\sigma = 7.5$, using only the short-time part of $S(q,t)$ for the fit ($t < 0.2\ \tau_I$, where $\tau_I = \sigma^2/4D_0$). In contrast, for patchy colloids, the short-time diffusion coefficient was determined by a stretched exponential fit to the initial decay of the ISFs ($t < 0.6\ \tau_I$). By fitting a similar stretched exponential function to the ISFs of colloids with only isotropic interactions, we confirmed that the fit function is not altering the diffusion coefficient.

For the centrosymmetric potentials, phase diagrams and critical temperatures were determined by Gibbs ensemble Monte Carlo (GEMC) simulations. For the patchy colloids, the Gibbs ensemble simulation results were inconclusive in determining a full phase boundary. The relatively small patch sizes lead to a very slow relaxation of the system by reorientation of the particles. Moreover, the strong patch-patch attractions resulted in a very large scatter of the simulation data for various system sizes and densities. However, at the temperature relevant to the dynamical simulations, we have found no indication for phase separation in the GEMC simulation nor in additional NVT simulations at that temperature. The calculated isotherms monotonously increased with the density. Structure factors calculated for low densities ($\phi < 0.05$) and extrapolated to zero-wave vector nicely follow the prediction from the isothermal compressibility using the low-density virial expression. These simulations yielded the values for B_2^* presented in Table 1.

SUPPLEMENTARY MATERIALS

Supplementary material for this article is available at http://advances.sciencemag.org/cgi/content/full/2/12/e1601432/DC1

movie S1. Transient cluster formation for particles with short-range attractions corresponding to snapshot in Fig. 3A.

movie S2. Transient cluster formation for particles with attractive patches corresponding to snapshot in Fig. 3B.

REFERENCES AND NOTES

1. R. J. Ellis, Macromolecular crowding: An important but neglected aspect of the intracellular environment. *Curr. Opin. Struct. Biol.* **11**, 114–119 (2001).
2. D. Hall, A. P. Minton, Macromolecular crowding: Qualitative and semiquantitative successes, quantitative challenges. *Biochim. Biophys. Acta* **1649**, 127–139 (2003).
3. G. B. Ralston, Effects of "crowding" in protein solutions. *J. Chem. Educ.* **10**, 857–860 (1990).
4. H.-X. Zhou, G. Rivas, A. P. Minton, Macromolecular crowding and confinement: Biochemical, biophysical, and potential physiological consequences. *Annu. Rev. Biophys.* **37**, 375–397 (2008).
5. S. B. Zimmerman, A. P. Minton, Macromolecular crowding: Biochemical, biophysical, and physiological consequences. *Annu. Rev. Biophys. Biomol. Struct.* **22**, 27–65 (1993).
6. T. Ando, J. Skolnick, Crowding and hydrodynamic interactions likely dominate in vivo macromolecular motion. *Proc. Natl. Acad. Sci. U.S.A.* **107**, 18457–18462 (2010).
7. S. R. McGuffee, A. H. Elcock, Diffusion, crowding & protein stability in a dynamic molecular model of the bacterial cytoplasm. *PLOS Comput. Biol.* **6**, e1000694 (2010).
8. A. Miermont, F. Waharte, S. Hu, M. N. McClean, S. Bottani, S. Léon, P. Hersen, Severe osmotic compression triggers a slowdown of intracellular signaling, which can be explained by molecular crowding. *Proc. Natl. Acad. Sci. U.S.A.* **110**, 5725–5730 (2013).
9. M. Weiss, Crowding, diffusion, and biochemical reactions. *Int. Rev. Cell Mol. Biol.* **307**, 383–417 (2014).
10. F. Mezei, Neutron spin echo: A new concept in polarized thermal neutron techniques. *Z. Phys. A-Hadron. Nucl.* **255**, 146–160 (1972).
11. F. Cardinaux, E. Zaccarelli, A. Stradner, S. Bucciarelli, B. Farago, S. U. Egelhaaf, F. Sciortino, P. Schurtenberger, Cluster-driven dynamical arrest in concentrated lysozyme solutions. *J. Phys. Chem. B* **115**, 7227–7237 (2011).
12. M. Grimaldo, F. Roosen-Runge, F. Zhang, T. Seydel, F. Schreiber, Diffusion and dynamics of γ-globulin in crowded aqueous solutions. *J. Phys. Chem. B* **118**, 7203–7209 (2014).
13. W. Häussler, Neutron spin echo studies on ferritin: Free-particle diffusion and interacting solutions. *Eur. Biophys. J.* **37**, 563–571 (2008).
14. C. LeCoeur, S. Longeville, Microscopic protein diffusion at high concentration by neutron spin-echo spectroscopy. *Chem. Phys.* **345**, 298–304 (2008).
15. F. Roosen-Runge, M. Hennig, T. Seydel, F. Zhang, M. W. A. Skoda, S. Zorn, R. M. J. Jacobs, M. Maccarini, P. Fouquet, F. Schreiber, Protein diffusion in crowded electrolyte solutions. *Biochim. Biophys. Acta* **1804**, 68–75 (2010).
16. A. Lawlor, G. D. McCullagh, E. Zaccarelli, G. Foffi, K. A. Dawson, Interactions in systems with short-range attractions and applications to protein crystallisation. *Prog. Coll. Pol. Sci.* **123**, 104–109 (2004).
17. W. C. K. Poon, Crystallization of globular proteins. *Phys. Rev. E* **55**, 3762–3764 (1997).
18. A. Stradner, G. M. Thurston, P. Schurtenberger, Tuning short-range attractions in protein solutions: From attractive glasses to equilibrium clusters. *J. Phys: Condens. Mat.* **17**, S2805–S2816 (2005).
19. G. Foffi, G. Savin, S. Bucciarelli, N. Dorsaz, G. M. Thurston, A. Stradner, P. Schurtenberger, Hard sphere-like glass transition in eye lens α-crystallin solutions. *Proc. Natl. Acad. Sci. U.S.A.* **111**, 16748–16753 (2014).
20. S. Bucciarelli, L. Casal-Dujat, C. De Michele, F. Sciortino, J. Dhont, J. Bergenholtz, B. Farago, P. Schurtenberger, A. Stradner, Unusual dynamics of concentration fluctuations in solutions of weakly attractive globular proteins. *J. Phys. Chem. Lett.* **6**, 4470–4474 (2015).
21. P. Schurtenberger, R. A. Chamberlin, G. M. Thurston, J. A. Thomson, G. B. Benedek, Observation of critical phenomena in a protein-water solution. *Phys. Rev. Lett.* **63**, 2064–2067 (1989).
22. P. N. Pusey, in *Neutrons, X-rays and Light: Scattering Methods Applied to Soft Condensed Matter,* P. Linder, T. Zemb, Eds. (Elsevier, 2002), pp. 203–220.
23. A. J. Banchio, G. Nägele, Short-time transport properties in dense suspensions: From neutral to charge-stabilized colloidal spheres. *J. Chem. Phys.* **128**, 104903 (2008).
24. F. Roosen-Runge, M. Hennig, F. Zhang, R. M. J. Jacobs, M. Sztucki, H. Schober, T. Seydel, F. Schreiber, Protein self-diffusion in crowded solutions. *Proc. Natl. Acad. Sci. U.S.A.* **108**, 11815–11820 (2011).
25. G. Gompper, T. Ihle, D. M. Kroll, R. G. Winkler, Multi-particle collision dynamics: A particle-based mesoscale simulation approach to the hydrodynamics of complex fluids. *Adv. Polym. Sci.* **221**, 1–87 (2009).
26. S. A. Rice, R. Kapral, Multiparticle collision dynamics: Simulation of complex systems on mesoscales. *Adv. Chem. Phys.* **140**, 89–146 (2008).
27. G. A. Vliegenthart, H. N. W. Lekkerkerker, Predicting the gas–liquid critical point from the second virial coefficient. *J. Chem. Phys.* **112**, 5364–5369 (2000).
28. G. Foffi, F. Sciortino, On the possibility of extending the noro–frenkel generalized law of correspondent states to nonisotropic patchy interactions. *J. Phys. Chem. B* **111**, 9702–9705 (2007).
29. A. Lomakin, N. Asherie, G. B. Benedek, Aeolotopic interactions of globular proteins. *Proc. Natl. Acad. Sci. U.S.A.* **96**, 9465–9468 (1999).
30. G. M. Thurston, Liquid-liquid phase separation and static light scattering of concentrated ternary mixtures of bovine α and γ*B* crystallins. *J. Chem. Phys.* **124**, 134909 (2006).
31. J. Z. Xia, Q. Wang, S. Tatarkova, T. Aerts, J. Clauwaert, Structural basis of eye lens transparency: Light scattering by concentrated solutions of bovine α-crystallin proteins. *Biophys. J.* **71**, 2815–2822 (1996).
32. S. Finet, A. Tardieu, α-crystallin interaction forces studied by small angle x-ray scattering and numerical simulations. *J. Cryst. Growth* **232**, 40–49 (2001).
33. P. Schleger, B. Alefeld, J. F. Barthelemy, G. Ehlers, B. Farago, P. Giraud, C. Hayes, A. Kollmar, C. Lartigue, F. Mezei, D. Richter, The long-wavelength neutron spin-echo spectrometer IN15 at the Institut Laue-Langevin. *Physica B* **241–243**, 164–165 (1997).
34. O. Holderer, M. Monkenbusch, R. Schätzler, H. Kleines, W. Westerhausen, D. Richter, The JCNS neutron spin-echo spectrometer J-NSE at the FRM II. *Meas. Sci. Technol.* **19**, 034022 (2008).
35. S. Poblete, A. Wysocki, G. Gompper, R. G. Winkler, Hydrodynamics of discrete-particle models of spherical colloids: A multiparticle collision dynamics simulation study. *Phys. Rev. E Stat. Nonlin. Soft Matter Phys.* **90**, 033314 (2014).

Acknowledgments: This work is based on experiments performed at the J-NSE instrument operated by the JCNS at the Heinz MLZ, Garching, Germany, and at the IN15 at ILL, Grenoble, France (experiment 9-13-390). **Funding:** This research project has been supported by the European Commission under the 7th Framework Programme through the Research Infrastructures Action of the Capacities Programme, NMI3-II (grant agreement number 283883). We gratefully acknowledge financial support from the Swiss National Science Foundation (grant 200020-127192), the Swedish Research Council (VR; grants 621-2012-2422 and 2009-6794), the Crafoord Foundation (grants 20120619 and 20140756), the Faculty of Science at Lund University, the European Research Council (ERC-339678-COMPASS), and the Knut and Alice Wallenberg Foundation (project grant KAW 2014.0052). A CPU time grant by the Jülich Supercomputer Center is also gratefully acknowledged. **Author contributions:** A.S. and P.S. designed the experimental study; S.B. purified the proteins and prepared the samples; S.B., B.F., O.H., P.S., and A.S. performed the NSE experiments; S.B. conducted the SAXS experiments; S.B., P.S., and A.S. analyzed the experimental data; R.G.W., G.A.V., and G.G. designed the simulation study; S.D., J.S.M., G.A.V., and R.G.W. performed and analyzed the simulations; and S.B., P.S., G.G., R.G.W., and A.S. jointly wrote the paper. **Competing interests:** The authors declare that they have no competing interests. **Data and materials availability:** All data needed to evaluate the conclusions in the paper are present in the paper and/or the Supplementary Materials. Additional data related to this paper may be requested from the authors.

Submitted 23 June 2016
Accepted 3 November 2016
Published 7 December 2016
10.1126/sciadv.1601432

Citation: S. Bucciarelli, J. S. Myung, B. Farago, S. Das, G. A. Vliegenthart, O. Holderer, R. G. Winkler, P. Schurtenberger, G. Gompper, A. Stradner, Dramatic influence of patchy attractions on short-time protein diffusion under crowded conditions. *Sci. Adv.* **2**, e1601432 (2016).

Dramatic influence of patchy attractions on short-time protein diffusion under crowded conditions

Saskia Bucciarelli, Jin Suk Myung, Bela Farago, Shibananda Das, Gerard A. Vliegenthart, Olaf Holderer, Roland G. Winkler, Peter Schurtenberger, Gerhard Gompper and Anna Stradner (December 7, 2016)

Sci Adv 2016, 2:.
doi: 10.1126/sciadv.1601432